Journal of Non-Crystalline Solids 358 (2012) 1958–1961

Contents lists available at SciVerse ScienceDirect

Journal of Non-Crystalline Solids

journal homepage: www.elsevier.com/ locate/ jnoncrysol

Origin of the V_{oc} enhancement with a p-doped nc-SiOx:H window layer in n-i-p solar cells

Rémi Biron *, Céline Pahud, Franz-Josef Haug, Christophe Ballif

Ecole Polytechnique Fédérale de Lausanne (EPFL), Institute of Microengineering (IMT), Photovoltaics and Thin Film Electronics Laboratory, 2000 Neuchâtel, Switzerland

ARTICLE INFO

Article history:
Received 31 July 2011
Received in revised form 23 January 2012
Available online 8 March 2012

Keywords:
Thin film silicon solar cell;
Off-stoichiometric silicon oxide;
Open-circuit voltage;
Built-in voltage

ABSTRACT

The introduction of a nc-SiOx:H material as window layer in single junction a-Si:H n-i-p solar cell leads to a V_{oc} enhancement of 80 mV compared to a μc-Si:H p-layer. According to numerical modeling of the V_{oc}, both the higher work function p-layer and the conduction band offset (CBO) at the i/p interface match well with the experimental V_{oc} increase with the oxygen content. Using the differential temperature method, the built-in voltage (V_{bi}) of the cells with the two different p-layers is measured to be similar, agreeing well with the CBO model. Thus we attribute the improvement of the V_{oc} to the reduction of recombination at the i/p interface, as a consequence of the CBO in this region.

1. Introduction

In amorphous silicon solar cells, the open-circuit voltage (V_{oc}) is one of the most ill understood parameters. The V_{oc} is intimately linked to the built-in voltage (V_{bi}) which is generally viewed as the upper limit of the V_{oc}. Many groups reported that the V_{oc} is improved by reducing the recombination at the i/p interface with the introduction of carbide [1,2] and graded boron [3] buffer layers. The numerical model proposed by Jiang et al. [4] predicts that the conduction band discontinuity at the i/p interface mitigates the thermionic emission process of electrons through the interface. These results suggest that V_{oc} is limited by recombination at the i/p interface rather than bulk recombination, contrary to the model of Hack and Shur [5]. We can also expect a higher V_{oc} by increasing the work function of the p-layer ϕ(p) which should increase the V_{bi} of the device, but thus necessitates also a front electrode with a higher work function. Few contributions discuss the V_{bi} enhancement at i/p interface brought by a higher ϕ(p) [6].

V_{oc} has been successfully improved with the use of wide band gap off-stoichiometric silicon oxide as window layer in a-Si:H [7,8] and μc-Si:H single junction solar cells [9,10]. In the latter case, Cuony et al. [9] attribute this improvement to the shunt quenching effect but it appears that it is not the dominant effect in the case of a-Si:H n-i-p solar cells as reported by Biron et al. [11]. Other groups reported that SiOx:H layers fabricated by glow discharge deposition from a SiH_4-CO_2-H_2 precursor gas mixture lead to the formation of a mixed phase (MP) material in which silicon nanocrystals are embedded into an a-SiOx:H matrix [12,13], instead of an amorphous Si–O compound corresponding to the random network model (RNM) [14,15].

In this paper, we present two models explaining the V_{oc} enhancement brought by the nc-SiOx materials in n-i-p solar cells. We correlate the V_{oc} improvement to the V_{bi} of the device, the electrical transport at the i/p interface and eventually to the p-layer microstructure.

2. Theory and calculation

The numerical models were computed using the one-dimensional (1-D) simulation package Advanced Semiconductor Analysis (ASA) developed at Delft University of Technology [16]. The dangling bond defect states around the midgap are modeled by the defect pool model proposed by Powell and Deane [17].

The values of the main input parameters are presented in the appendix. The numerical analysis describes the modeling of the V_{oc} variation with the oxygen content in the p-layer by varying its mobility band gap E_g, electron affinity χ and activation energy E_a. Thus ϕ(p), V_{bi} and the CBO at the i/p interface (ΔEc) can be tuned according to the following formula:

$$\phi(p) = \chi(p) + E_g(p) - E_a(p) \quad (1)$$

$$V_{bi} = \phi(p) - \phi(n) \quad (2)$$

$$\Delta E_C = \chi(p) - \chi(i) \quad (3)$$

In the MP SiOx:H material, Watanabe et al. observe that the microstructure of the O-rich region can be described by the RNM [12]. Thus we assume that the a-SiOx:H matrix surrounding the silicon nanoclusters can be described by this model. We also assume that this

* Corresponding author. Tel.: +41 32 718 32 19.
E-mail address: remi.biron@epfl.ch (R. Biron).
URL: http://pvlab.epfl.ch/ (R. Biron).

0022-3093/$ – see front matter © 2012 Elsevier B.V. All rights reserved.
doi:10.1016/j.jnoncrysol.2012.01.058

phase is mainly present at the i/p interface, governing the electrical transport in this region.

We deposit the p-layer in two steps p1 and p2. In the first step, oxygen is added via the CO_2 flux into the deposition gas mixture. The amount of oxygen into the p1 layer is tuned by varying the CO_2 flux. In the second step, no oxygen is incorporated. The stack for the models is thus n-layer/i-layer/p1-layer/p2-layer. Only the band structure of the p1-layer is changed because of the tunable oxygen content. p2 is assumed to be μc-Si:H. In numerical analyses, the oxygen incorporation in the a-Si:H matrix is modeled by the linear increase of E_g, as reported for randomly bonded a-SiOx:H layers [18,19]. For the oxygen content varying from 0% to 26%, E_g linearly increases from 1.81 to 2.11 eV as shown in Fig. 2, whereas E_a of purely amorphous SiOx:H varies between 0.37 eV and 0.50 eV, agreeing with the values reported for a-SiOx p-layers [20]. In the first model, χ is kept constant, leading to an increase of ϕ(p). Thus it produces a higher V_{bi} in the device according to the formula (2). We call this model "V_{bi} enhancement model." In the second model, χ(p) is reduced when oxygen in added, compensating the gain in the E_g–E_a difference. It results in a CBO at the i/p interface, ΔEc, according to the formula (3) which increases with the oxygen content. Thus the V_{bi} is kept constant over the E_g range (formula (1) and (2)). We refer this model to "CBO model." The evolution of V_{bi} and χ(p) with E_g for both models is presented in Fig. 1.

For the V_{bi} determination, we use the differential temperature method (DTM) proposed by Hegedus [6], using a one-diode model for the description of a single junction solar cell. The V_{oc}–lnJ_{sc} data are fitted according to the following equation:

$$V_{oc} = nkT/q \ln(J_{sc}/J_0) \quad (4)$$

where n is the ideality factor of the diode, k the Boltzmann constant, T the temperature in Kelvin, q the elementary charge, J_{sc} the current density in short-circuit condition and J_o the saturation current. The V_{bi} is calculated according to the following formula:

$$\frac{V_{oc}(T_1)}{n(T_1)}\left[\frac{T_2}{T_2-T_1}\right] - \frac{V_{oc}(T_2)}{n(T_2)}\left[\frac{T_1}{T_2-T_1}\right] \quad (5)$$

3. Experimental

The solar cell fabrication and layer characterization were the same as in a previous publication [11]. The p-nc-SiO_x reference layers were deposited on glass by very high frequency plasma enhanced chemical vapor deposition (VHF-PECVD) at 70 mHz and 0.4 mbar, with a gas mix of SiH_4, H_2, CO_2 and trimethyl borane (TMB, $B(CH_3)_3$) for the doping gas. The power density used was around 100 mW per cm^2 and the deposition temperature was 190°C. Films were deposited to be 60 nm thick. The dilution ratio and the doping ratio $[B(CH_3)_3]/[SiH_4]$ were kept constant at 130 and 0.01, respectively.

In order to characterize the dependency of the p-layer microstructure to the oxygen content, both planar conductivity (σ_{RT}) and activation energy (E_{act}) were determined by dark conductivity measurements.

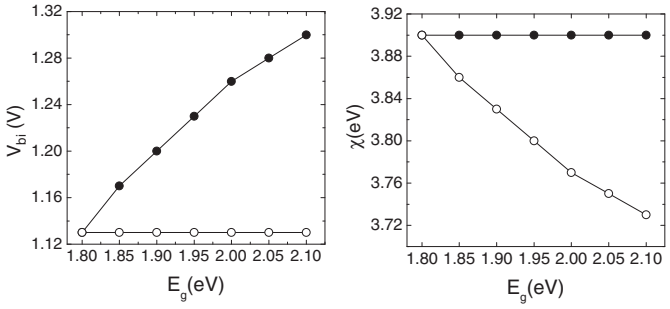

Fig. 1. Variation of the V_{bi} and χ(p) with E_g for both the "V_{bi} enhancement" (full circles) and "CBO" (open circles) models.

The crystallinity of the films was measured by Raman spectroscopy. The crystallite size was assessed by X-ray diffractometry.

The optical band gap E_{04} and the Tauc band gap E_g were extracted from ellipsometry measurements. The oxygen content was investigated by Fourier transform infrared absorption measurements, using the quantitative data analysis of He et al.[21].

The n-i-p solar cells were deposited on glass covered with a back contact of 2 μm thick ZnO films deposited by low-pressure chemical vapor deposition (LP-CVD) [22]. The silicon layers were deposited by PE-CVD at the same temperature and pressure as mentioned above.

The intrinsic layer was about 250 nm thick with a $[H_2]/[SiH_4]$ ratio of two. For the 20 nm thick p1-layers, we used the same conditions as the reference layers with $[CO_2]/[SiH_4] = 0$ and 2. Another LP-CVD ZnO layer was deposited as front electrode.

For the cell characterization, we performed current–voltage (I–V) measurements under a simulated AM1.5 spectrum and external quantum efficiency (EQE) measurements in their initial state.

The V_{bi} voltage of the solar cells was determined by DTM. To determine the ideality factor n, we performed the variable illumination measurement (VIM) at 7 different illuminations ranging from 0.4% to 100% of the AM 1.5 G illumination by using color neutral filters. We extracted the n value after fitting the J_{sc}-V_{oc} curves with the one-diode model under illumination. Then the VIM was performed at 3 different temperatures (303, 333, and 363 K) in order to calculate the V_{bi}.

4. Results

Fig. 2 shows the microstructure and the electrical properties of the p-layers with the oxygen content. The graph on the left illustrates that the oxygen content increases roughly linearly with the $[CO_2]/[SiH_4]$ ratio. The main uncertainty in the oxygen content is the quantitative analysis of the FTIR spectra. The incorporation of oxygen in the H-diluted p-layer leads to the linear widening of the Tauc band gap from 1.81 to 2.29 eV while E_a increases slowly from 0.053 to 0.197 eV for oxygen content lower than 26% before deteriorating strongly up to 0.740 eV for the highest oxygen content. The errors in E_a calculation correspond to the choice of the temperature range on the Arrhenius plot. For the E_g calculations, the Chi square values resulting from the fits of the ellipsometry data are 2.82, 1.27, 4.5, 4.9 and 0.72 for E_g equal to 1.81, 1.95, 2.04, 2.11 and 2.29, respectively. The error bars are the distribution corresponding to three different sets of measurement. The crystallite sizes deduced from XRD measurements decrease progressively from 19 nm for the O-free p-layer to 9 nm for the 6% O-rich layer. Then the crystallite size tends to the zero towards more O-rich films, pointing out that films become more amorphous. This trend is consistent with the Si-Raman crystallinity fraction which drops from 53 to 11.5% with the addition of oxygen. The mains errors in the XRD size and the Si-Raman crystallinity measurements come from the resolution of the technique (2–3 nm) and the scattering of the measurements, respectively.

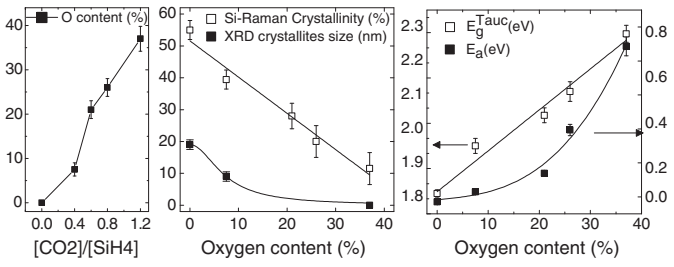

Fig. 2. Incorporation of oxygen into the films in function of the $[CO_2]/[SiH_4]$ ratio (left). XRD sizes of silicon nanograins and Si-Raman crystallinity as a function of the oxygen content (center). Evolution of E_a and the Tauc bandgap E_g with the oxygen content(right).

In Fig. 3, the experimental V_{oc} trend of our previous contribution is included [11]. The error in the V_{oc} measurements shown in this contribution is ±5 mV due to the uncertainty of the substrate temperature. The evolution of the computed V_{oc} when E_g of the p-layer increases is also plotted. The "V_{bi} enhancement model" yields a progressive increase of V_{oc} up to 0.925 V for E_g=1.95 eV, following roughly V_{bi} plotted in Fig. 1. The increasing can be explained by the higher electric field in the i-layer close to the interface shown in Fig. 3 (band diagram on the left). Beyond E_g = 1.95 eV, it rapidly decreases to the value of 0.87 V, although the V_{bi} still increases as shown in Fig. 1. Similar behavior is obtained for the "CBO model," where V_{oc} increases up to E_g=2.0 eV with a less pronounced drop after the maximum point. In this case the gain in V_{oc} agrees well with the increasing ΔEc (seen in Fig. 1, band diagram on the right) created by a reduced χ_p seen in Fig. 1. Indeed ΔEc at the i/p interface limits the injection of photogenerated electrons into the p-layer, decreasing recombination. We note that both computed V_{oc} variations agreed with the increase of the experimental V_{oc} trend for E_g up to 1.95 eV. Nevertheless, for higher E_g values, the V_{oc} trend obtained with the "CBO model" fits better with the experimental values because the V_{oc} decrease in less pronounced. In the case of the "V_{bi} enhancement model," the stronger V_{oc} drop can be explained by the bigger increase of the barrier height in the valence band at the i-a-Si:H/p-nc-SiOx:H interface seen in Fig. 3. For the highest oxygen content, this barrier becomes critically higher so that the hole transfer into the p-layer is disturbed. Then their possible recombination with photogenerated electrons should reduce the V_{oc}.

Fig. 4 shows the V_{oc}–lnJ_{sc} measurements of cells A and B with the μc-Si:H and nc-SiOx:H p-layers, respectively, at three different temperatures. The slope observed for the cell with the nc-SiOx:H p-layer is higher compared to the O-free p-layer over the temperature range, indicating that the ideality factor is bigger according to equation (4). It is calculated to be 1.46, 1.47 and 1.42 at 303, 333, and 363 K, respectively while the cells with the O-free p-layer exhibit values of 1.23, 1.22, and 1.19, revealing that n is slightly temperature dependant. It is also noted that V_{oc} of the cell with the nc-SiOx:H p-layer remains at higher values. The V_{bi} calculated by DTM is show in Fig. 4 (graph on the left). One pair of temperature is needed to calculate the V_{bi} as shown by the equation (5). Two sets of V_{bi} values are eventually calculated, i.e. one set

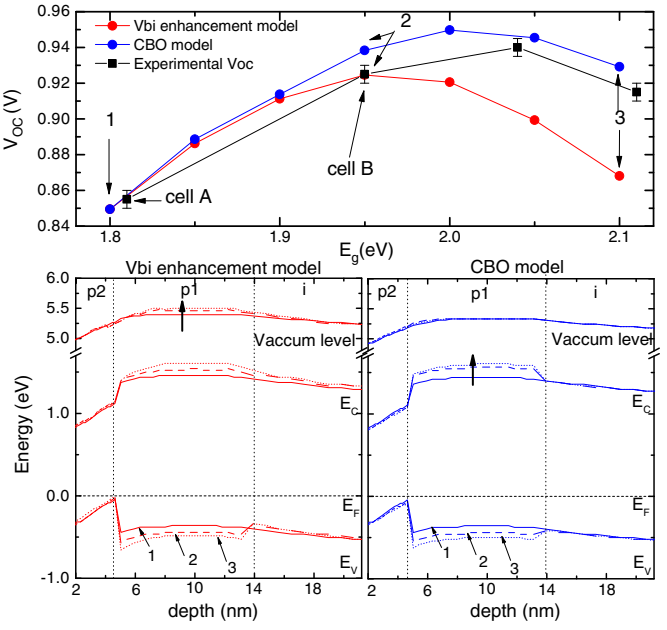

Fig. 3. Experimental and modeled V_{oc} (Top part). Cells A and B are taken for the V_{bi} measurement (see Fig. 4). Bottom part: energy band diagrams in thermal equilibrium for the "V_{bi} enhancement model" (left) and the "CBO model" (right). The zero energy is the Fermi level. The situations 1, 2 and 3 correspond to the minimum, optimum and maximum E_g, respectively.

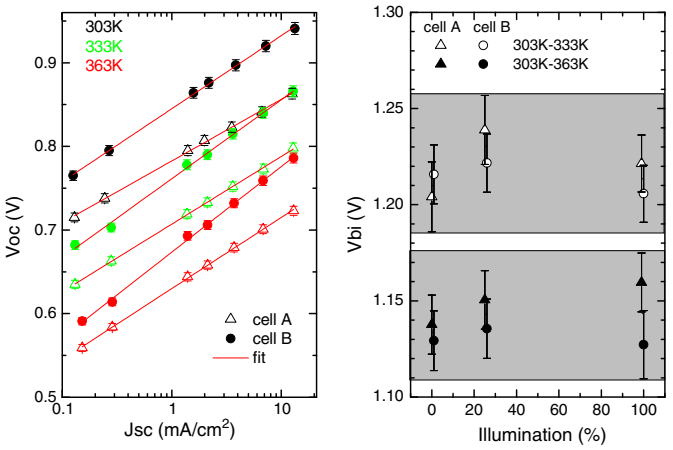

Fig. 4. V_{oc}–lnJ_{sc} data of cells A and B at different temperatures (left part), with the p-μc-Si:H (triangles) and p-nc-SiOx:H layers (circles), respectively. Right part: measured DTM V_{bi} of cells A and B at different illuminations and for different pairs of temperature (see formula (5)). For further information, refer to the contribution of Hegedus [6].

corresponding to the pair 303–333 K (upper grey bar) and the other one to the pair 303–363 K (lower grey bar) that we call "cold" V_{bi} and "hot" V_{bi}, respectively. Thus the comparison of the V_{bi} of both cells A and B has to be made for each set of V_{bi}. The V_{bi} calculation was also performed at three different illuminations, i.e. 1, 25 and 100% of the AM 1.5 g illumination. The graph shows that over the illumination range, the "cold" V_{bi} values range from 1.20 to 1.24 V and from 1.21 to 1.22 V for cell A and cell B, respectively. The "hot" V_{bi} values are lower, ranging from 1.14 to 1.16 V and from 1.15 to 1.18 V for cell A and cell B, respectively. According to these results, it appears that the V_{bi} is slightly influenced by the illumination but affected strongly by the temperature. The error in the V_{bi} is a composite of the errors in the n value calculation, the substrate temperature and the Voc measurements. We evaluate the scattering of V_{bi} values which is 77 and 67 mV for the "cold" and "hot" V_{bi} sets, respectively.

5. Discussion

First we found that our films present silicon nanocrystals embedded in the a-SiOx:H matrix according to XRD and Si-Raman crystallinity measurements seen in Fig. 2. The introduction of oxygen in the hydrogen-diluted p-layer tends to delay the growth of silicon nanocrystals, suggesting that an a-SiOx:H phase primarily grows at the i/p interface.

Then we discuss the validity of the numerical models in respect with the experimental V_{oc} trend with the oxygen content and the DTM V_{bi}. In Section. 2, it was assumed that the p-doped a-SiOx:H phase governs the electrical transport. This assumption is supported by the agreement between the numerical and the experimental enhancement of the V_{oc}. In our work, both models are discriminated by two set of results, i.e. the computed V_{oc} trends obtained from both models and the experimental V_{bi} values determined by DTM. First, simulation results show that the V_{oc} trend predicted by the "CBO" model follows better the experiment. Secondly, we observed that the V_{bi} increase of 170 mV predicted by the "V_{bi} enhancement" is not observed experimentally since the scattering of both sets of V_{bi} shown in Fig. 4 is even less than the half of the expected V_{bi} increase. These two arguments thus indicate that the V_{oc} improvement with the nc-SiOx:H p-layer could come from the change in the band structure at the i/p interface, resulting in a CBO, which in turn creates a field that impedes electrons to recombine with holes. The decrease of the V_{bi} for both types of cell shown in Fig. 4 is relatively strong compared to the results reported by Kaplan and Kaplan [28] who also determined the V_{bi} by DTM. In the literature we did not find contribution dealing with the explanation of the V_{bi} drop with the temperature. The argument of a CBO at the i/p interface is well consistent with the explanation of [27] for silicon carbide buffer layers. The presence

of the a-SiOx:H phase at the i/p interface, the simulation results and the constancy of the DTM V_{bi} are in good agreement with the "CBO model."

In addition to both models, we also evaluated another model where the mobility band gap of the p1-layer is increased by pushing towards lower energies the maximum of the valence band. But that model finally yields V_{oc} values lower that 0.8 eV. Other models are thinkable since both models assessed in this contribution do not take into account the presence of both μc-Si:H and a-SiOx:H phases forming the nc-SiO:H p-layer.

6. Conclusion

The numerical modeling of the i/p interface in n-i-p solar cells shows that two different scenarios lead to the enhancement of the V_{oc}. The first one consists in increasing the work function of the p-layer, enhancing the V_{bi} of the cell. The second model assumes a reduced p-layer electron affinity, yielding a conduction band discontinuity at the i/p interface that impedes electrons from recombining with holes in the p-layer. We favor the second model because it appears to fit better with the experiment. The a-SiOx:H phase in direct contact with the i-layer should be desirable to limit recombination, resulting in a higher V_{oc}.

Acknowledgements

We thankfully acknowledge funding by the European Union within the FP7 project Silicon-Light (contract no. 241277).

Appendix A

Table 1
The set of values for the band structure of the n-i-p a-Si:H single junction solar cell.

Parameters	n-layer	i-layer	p1-layer	p2-layer
Dielectric constant	11.9	11.9	11.9	12
Thickness (10^{-9} m)	20	200	10	5
Mobility gap E_g (eV)	1.8	1.8	1.8–2.1(1)	1.15
Electron affinity χ (eV)	3.9	3.9	3.9–3.73(1)	4.1
Activation energy E_a (eV)	0.3	0.9(2)	0.37–0.50(1)	0.05
Hole mobility in VB (10^{-4} m^2/V.s)	0.3(3)	2.0(3)	0.3(3)	0.7(4)
Electron mobility in CB (10^{-4} m^2/V.s)	15(3)	15(3)	5(3)	5(4)
Effective DOS in CB (m^{-3})	4e26	4e26	4e26	6e25
Effective DOS in VB (m^{-3})	4e26	4e26	4e26	3e25
Temperature (K)	300	300	300	300
Tails states parameters				
DOS at CB mobility edge (m^{-3}/eV)	7e27	4e27	1e28	1e28
DOS at VB mobility edge (m^{-3}/eV)	7e27	2e27	1e28	1e28
VB tail characteristic energy (eV)	0.060	0.045	0.090	0.070
CB tail characteristic energy (eV)	0.050	0.025	0.060	0.050
CR in neutral and charged states in CB (m^3/s)	1e−14	1e−14	2e−14	2e−14
CR in neutral and charged states in VB (m^3/s)	2e−14	2e−14	4e−14	4e−14
Length of the CB and VB tails (eV)	0.90	0.90	0.90	0.90
Defect states parameters (defect pool model(5))				
Standard deviation	0.195	0.188	0.195	–
Electron and hole CR of neutral DBs (m^3/s)	1e−15	1e−15	1e−15	1e−15
Electron and hole CR of charged DBs (m^3/s)	1e−14	1e−14	1e−14	1e−14
Pos. of the Gaussian defect pool (rel. to VB) (eV)	1.22	1.22	1.25	–

(1)The variations of these values are presented in Figs. 1 and 2.
(2)We assume that E_a corresponds to the Fermi level energy in the intrinsic layer. Thus it is the half of E_g.
(3)The values are consistent with the work of Spear [23] and Street et al. [24].
(4)The values are consistent with the work of Dylla et al. [25] and Dylla et al. [26].
(5)See ref. [17].

References

[1] H. Sakai, T. Yoshida, S. Fujikake, T. Hama, Y. Ichikawa, J. Appl. Phys. 67 (1990) 3494–3499.
[2] R.E. Rocheleau, S.S. Hegedus, W.A. Buchanan, S.C. Jackson, Appl. Phys. Lett. 51 (1987) 133–135.
[3] R.R. Arya, A. Catalano, R.S. Oswald, Appl. Phys. Lett. 49 (1986) 1089–1091.
[4] L. Jiang, J.H. Lyou, S. Ranea, E.A. Schiff, Q. Wang, Q. Yuana, Mater. Res. Soc. Proc., 609, 2000, A18, 3.1.
[5] M. Hack, M.S. Shur, J. Appl. Phys. 55 (1984) 4413–4417.
[6] S.S. Hegedus, Nineteenth IEEE Photovoltaic Specialists Conf. Proc, 1987, pp. 210–215.
[7] P. Sichanugrist, T. Sasaki, A. Asano, Y. Ichikawa, H. Sakai, Sol. Energy Mater. Sol. Cells 34 (1994) 415–422.
[8] K. Sriprapha, N. Sitthiphol, P. Sangkhawong, V. Sangsuwan, A. Limmanee, J. Sritharathikhun, Curr. Appl. Phys. 11 (2011) S47–S49.
[9] P. Cuony, M. Marending, D.T.L. Alexander, M. Boccard, G. Bugnon, M. Despeisse, C. Ballif, Appl. Phys. Lett. 97 (2010) 213502.
[10] T. Krajangsang, I. Yunaz, S. Miyajima, M. Konagai, Curr. Appl. Phys. 10 (2010) S357–S360.
[11] R. Biron, C. Pahud, F.-J. Haug, J. Escarre, K. Söderström, C. Ballif, J. Appl. Phys. 110 (2011) 124511.
[12] H. Watanabe, K. Haga, T. Lohner, J. Non-Cryst. Solids 164–166 (1993) 1085–1088.
[13] K. Haga, H. Watanabe, Jpn. J. Appl. Phys. 29 (1990) 636–639.
[14] F.G. Bell, L. Ley, Phys. Rev. B 37 (1988) 8383–8393.
[15] A. Singh, S. Bayliss, S. Gurman, E. Davis, J. Non-Cryst. Solids 142 (1992) 113–125.
[16] M. Zeman, J.A. Willemen, L.L.A. Vosteen, G. Tao, J.W. Metselaar, Sol. Energy Mater. Sol. Cells 46 (1997) 81–99.
[17] M.J. Powell, S.C. Deane, Phys. Rev. B 48 (1993) 10815–10827.
[18] E. Holzenkämpfer, F.-W. Richter, J. Stuke, U. Voget-Grote, J. Non-Cryst. Solids 32 (1979) 327–338.
[19] E. Martinez, F. Ynduráin, Phys. Rev. B 24 (1981) 5718–5725.
[20] A. Janotta, R. Janssen, M. Schmidt, T. Graf, M. Stutzmann, L. Görgens, A. Bergmaier, G. Dollinger, C. Hammerl, S. Schreiber, B. Stritzker, Phys. Rev. B 69 (2004) 115206.
[21] L.N. He, D.M. Wang, S. Hasegawa, J. Non-Cryst. Solids 261 (2000) 67–71.
[22] S. Faÿ, U. Kroll, C. Bucher, E. Vallat-Sauvain, A. Shah, Sol. Energy Mater. Sol. Cells 86 (2005) 385–397.
[23] W.E. Spear, J. Non-Cryst. Solids 59–60 (1983) 1–13.
[24] R.A. Street, J. Kakalios, M. Hack, Phys Rev. B 38 (1988) 1–13.
[25] T. Dylla, F. Finger, E.A. Schiff, Appl. Phys. Lett. 87 (2005) 032103.
[26] T. Dylla, S. Reynolds, R. Carius, F. Finger, J. Non-Cryst. Solids 352 (2006) 1093–1096.
[27] S.S. Hegedus, IEEE Photovoltaic Specialists Conf. Proc, 1988, pp. 210–215.
[28] R. Kaplan, B. Kaplan, Turk. J. Phys. 25 (2001) 375–383.